

Supporting Information for Edge-dominated Hydrogen Evolution Reactions in Ultra-narrow MoS₂ Nanoribbon Arrays

Ding-Rui Chen,^{a,b,c} Jeyavelan Muthu,^d Xing-You Guo,^e Hao-Ting Chin,^{a,b,c} You-Chen Lin,^a Golam Haider,^f Chu-Chi Ting,^e Martin Kalbáč,^f Mario Hofmann^d and Ya-Ping Hsieh^{*abc}

^a*Institute of Atomic and Molecular Sciences, Academia Sinica, Taipei, 10617, Taiwan*

^b*International Graduate Program of Molecular Science and Technology, National Taiwan University, Taipei, 10617, Taiwan*

^c*Molecular Science and Technology Program, Taiwan International Graduate Program, Academia Sinica, Taipei, 10617, Taiwan*

^d*Department of Physics, National Taiwan University, Taipei, 10617, Taiwan*

^e*Department of Mechanical Engineering, Institute of Opto-Mechatronics, National Chung Cheng University, Chiayi, 62301, Taiwan*

^f*J. Heyrovsky Institute of Physical Chemistry of the Czech Academy of Sciences, Prague, 18200, Czech Republic*

*Corresponding author Email: yphsieh@gate.sinica.edu.tw

Number of Pages: 20

Number of Figures: 13

Number of Tables: 3

Supplementary Figures

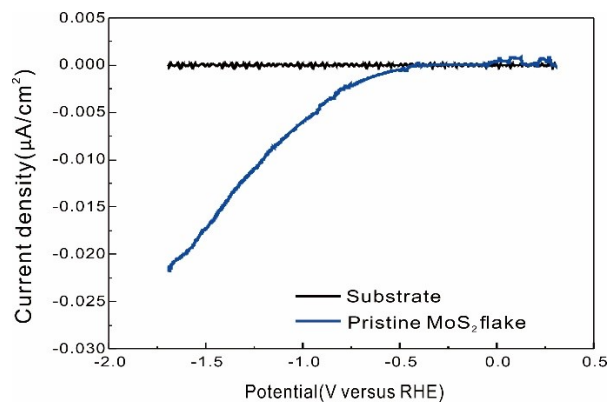


Fig. S1. The polarization curves of the substrate (Black curve) and pristine MoS_2 flake (blue curve).

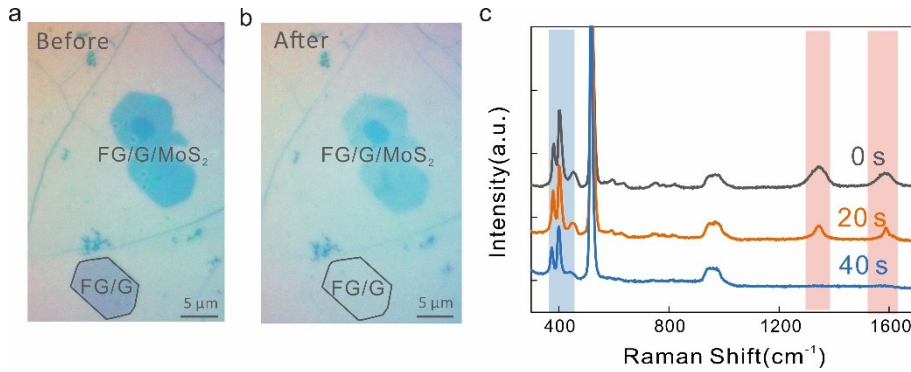


Fig. S2. After selective patterning, we obtained fluorographene/graphene/MoS₂ heterostructure (FG/G/MoS₂). To remove the etching mask, the fluorographene/graphene was etched for 40s by O₂ plasma. By locating specific regions before and after each process step, we performed carefully optical images and Raman spectroscopic measurements on the same region with FG/G and fluorographene/graphene/MoS₂. The disappearance of the fluorographene/graphene in the OM images (Fig. S2a and b) and the absence of the G band in the Raman spectrum, indicate the successful removal of the fluorographene. (Fig. S2c) Besides, the intensity peak for MoS₂ shows no changes, indicating the retention of MoS₂.

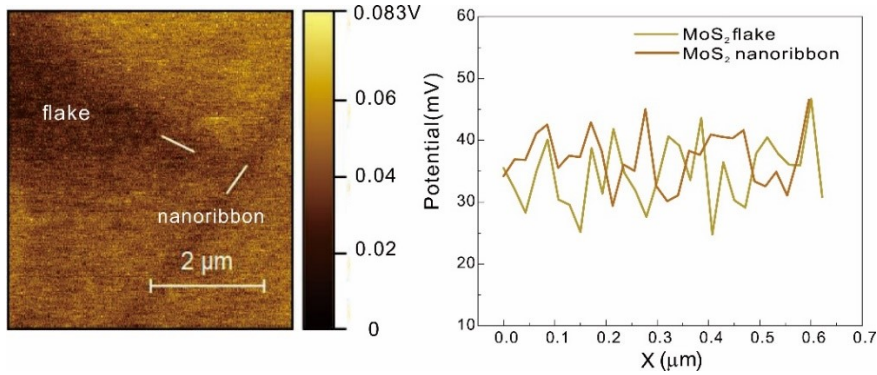


Fig. S3. To further confirm fluorographene/graphene nanomask is removed successfully, we used KPFM to characterize the surface potential distribution. The output image shows the potential difference (V_{cpd}) between the surface and the conductive tip. Prior to this measurement, work function of the metal tip (Φ_{tip}) is calibrated using gold film and found to be 5.01 eV. The work function of sample is extracted by the following formula:¹

$$V_{cpd} = (\phi_{tip} - \phi_{sample})/e \quad (1)$$

where ϕ_{tip} , ϕ_{sample} , e are the work function of tip, work function of sample and unit electron charge, respectively. Figure S3 shows comparable V_{cpd} for flake and nanoribbons at 42.9 mV and 38.7mV, representing work functions of 5.05 eV and 5.04 eV, respectivitely. The values are agree with previous reports² and are different from fluorographene and graphene.³

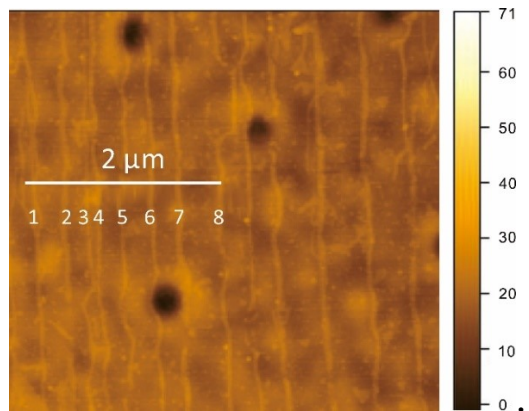


Fig. S4. Atomic force microscopy (AFM) imaging of aligned MoS₂ nanoribbons array revealed a density of $4\mu\text{m}^{-1}$.

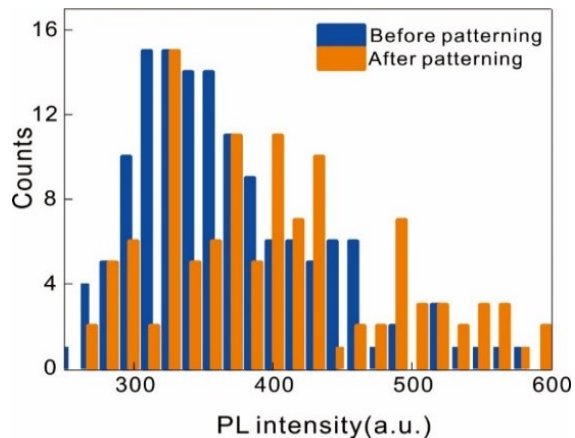


Fig. S5. To quantify the quality of thus patterning MoS₂ nanoribbons, the PL intensity distribution from before and after patterning was compared. The quality of MoS₂ nanoribbon does not deteriorate through further patterning as the intensity distribution is similar.

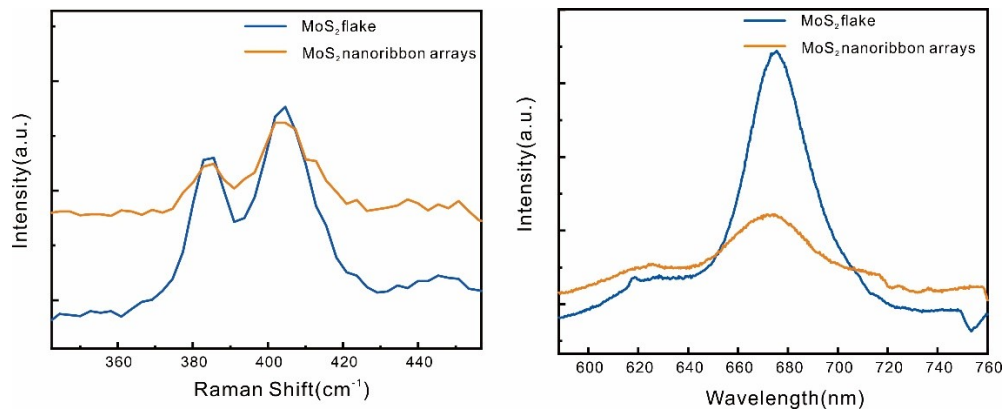


Fig. S6. Optical spectroscopy showing retention of quality after TSPP: (a) Raman spectroscopy with similar peak positions showing absence of strain, (b) Photoluminescence spectroscopy demonstrating similar trion-to-exciton ratio, corroborating the absence of additional charge transfer. Based on the demonstrated retention of the basal plane quality, changes in the electrochemical performance of nanoribbons have to originate from their edges.

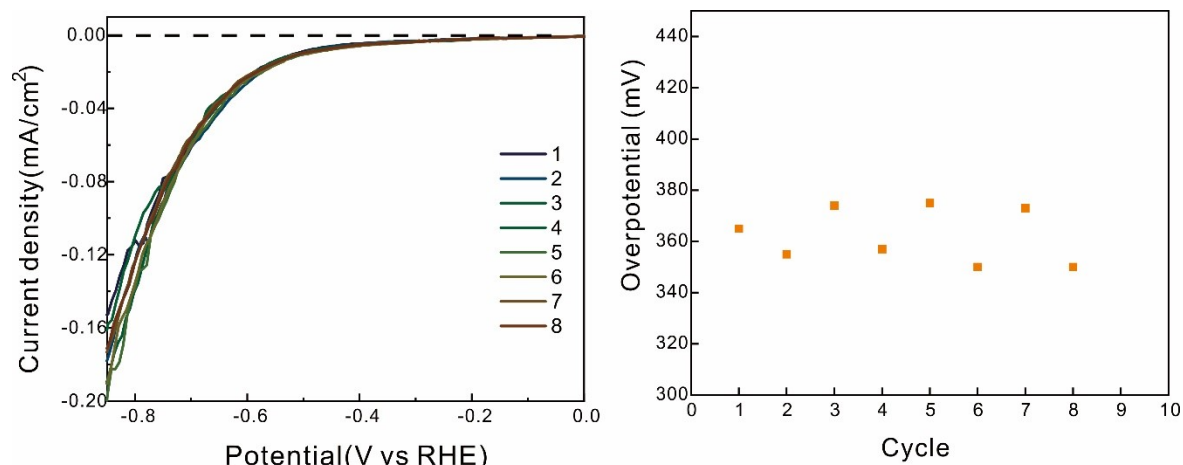


Fig. S7. Demonstration of HER reproducibility (a) Polarization curves for multiple sequential cycles, (b) extracted overpotential vs. cycle number showing no systematic change and a reproducibility of 350mV.

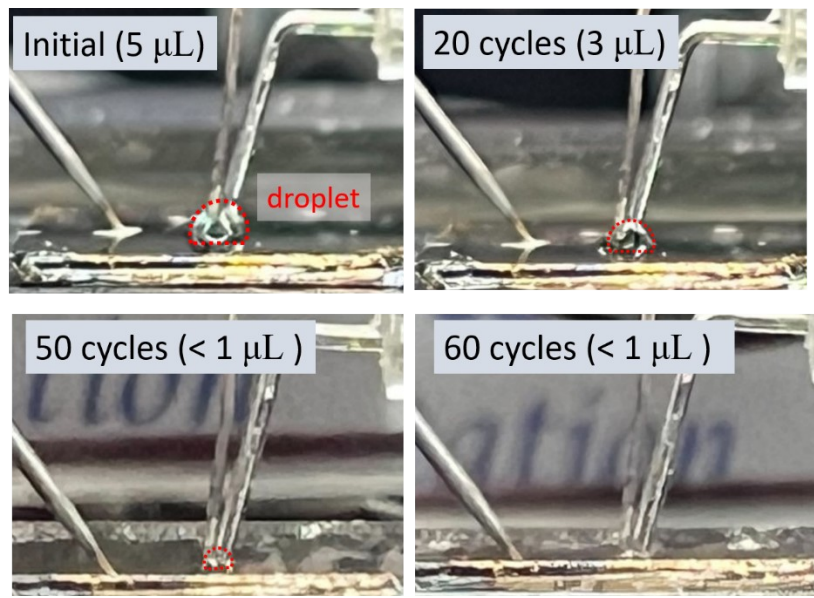


Fig. S8. After 50 cycles the volume of the droplet is insufficient to allow contact to all three electrodes which represents the limit of our experimental duration.

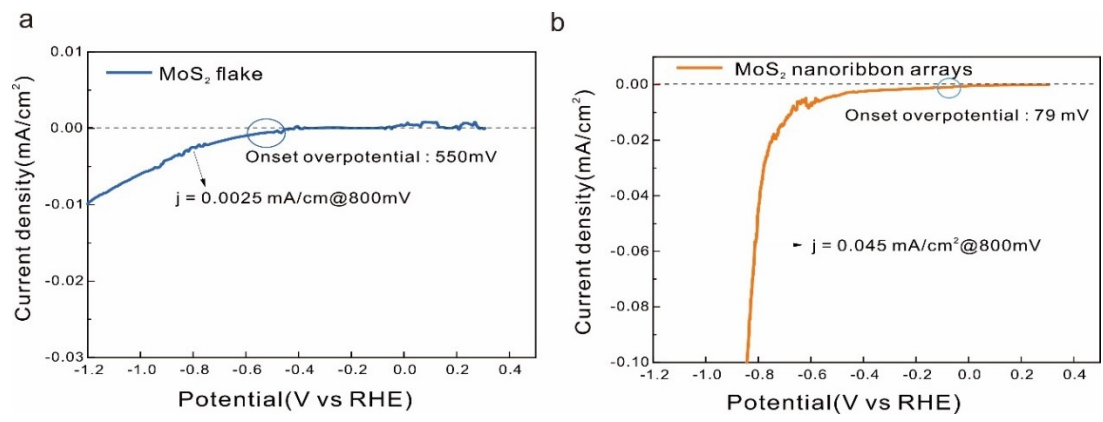


Fig. S9. The onset overpotential and the current density @800 mV of the (a)MoS₂ flake and (b)MoS₂ nanoribbon arrays were obtained from the polarization curves.

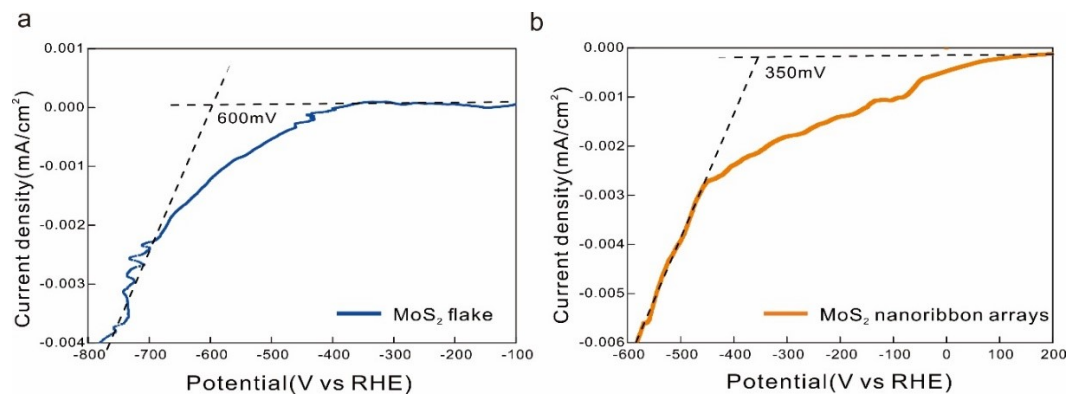


Fig. S10. The overpotential of the (a) MoS_2 flake and (b) MoS_2 nanoribbon arrays.

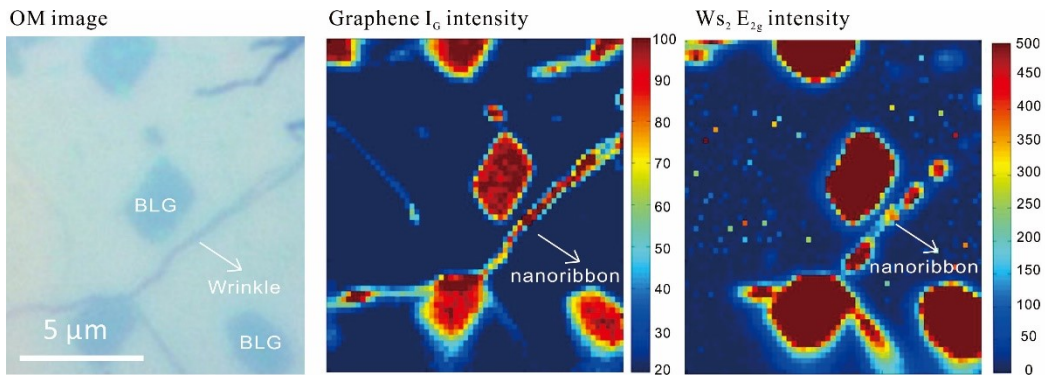


Fig. S11. The patterning process was further applied to create tungsten diselenide nanoribbons. Using the same process, graphene nanowrinkles were transferred to WS₂. The patterned samples were characterized by optical microscopy (OM) and Raman spatial map. With the CF₄ treatment, only bilayer graphene-protected WS₂ will remain. Similar to the scenario in MoS₂ case, the Raman features of WS₂ only remain in the bilayer-covered regions.

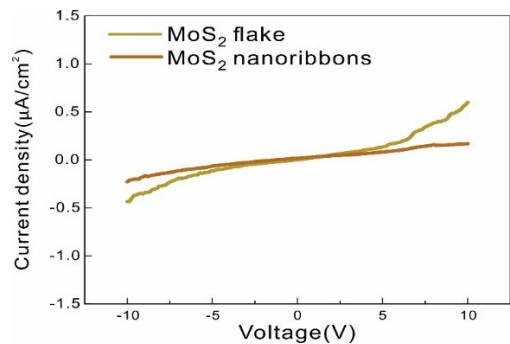


Fig. S12. Current-voltage characteristics of the MoS₂ flake and MoS₂ nanoribbons device.

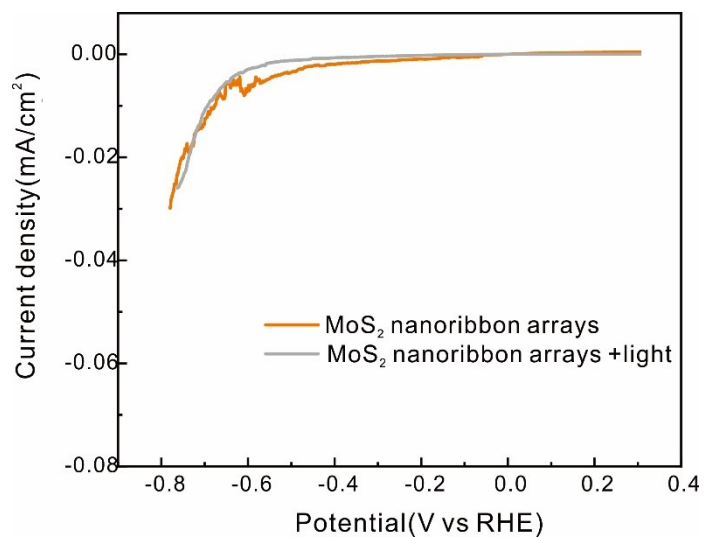


Fig. S13. Polarization curves for nanoribbons under illumination and dark conditions.

Supplementary Tables

Table S1. Overview of width and density of reported preparation strategies of MoS₂ nanoribbons. Some values are calculated by their AFM, SEM, and OM images in the studies.

material	strategy	width	ribbon density (number/100um)	reference
MoS ₂ nanoribbon	templated subtractive fabrication	20	400	Our work
	scanning probe lithography	30	50	4
	stamp-printing method.	130	400	5
	stamp-printing method.	135	150	6
	etching (Reactive Ion Etch)	250	60	7
	etching (solution)	300	10	8
	bottom-up direct growth (Ledge-directed epitaxy)	73	250	9
	bottom-up direct growth (NaOH-assisted VLS growth)	700	20	10
	bottom-up direct growth (Vapour–liquid–solid)	195	100	11

Table S2. Comparison Table showing the Tafel slope and exchange current enhancement of pristine 2H-MoS₂ and 2H-MoS₂ after modification strategies.

Strategy	Tafel slope (m Vdec ⁻¹)	exchange current increment ($\Delta J/J_0$) (estimated)	reference
our pristine MoS ₂	153	-	
templated subtractive fabrication (MoS ₂ nanoribbon arrays)	94	18	Our work
pristine	200	-	12
pristine	110	-	13
pristine	95	-	13
pristine	191	-	14
pristine	165	-	15
pristine	98	-	16
pristine	187	-	17
pristine	325	-	18
pristine	118	-	19
pristine	229	-	20
pristine	237	-	21
pristine	98	-	22
pristine	169	-	23
pristine	152	-	24
pristine	151	-	25
pristine	200	-	26
pristine	115	-	27
pristine	160	-	28
edge rich	136	5	12
edge rich	95	3	13
edge rich	96	10	14
edge rich	122	5	17
edge rich	109	11	17
edge rich	89	9	19
edge rich	163	12	20
edge rich	93	10	21
edge rich	79	4	23
atomic vacancies	105	8	15
atomic vacancies	90	2	16
atomic vacancies	67	5	22
atomic vacancies	86	3	29

atomic vacancies	102	12	25
annealing	89	15	15
annealing	117	6	18
plasma	108	9	30
plasma	105	10	30
plasma	171	11	18
utilizing the electric field	110	10	26
utilizing the electric field	100	8	27

Table S3. Comparison of exchange current density and turnover frequency (TOF) for our work with Pt, Hg, MoS₂ and MoSe₂ related materials.

Material	exchange current density (A/cm ²)	turnover frequency - TOF (S ⁻¹)	reference
pristine MoS ₂	9.7E-7	3E-3	Our work
MoS ₂ nanoribbon	2.2E-6	0.78	
Pt (111)	4.5E-4	0.94	
Hg	5E-13	1.04E-9	
MoS ₂ -edge	7.9E-6	1.64E-2	
vertical MoS ₂ aligned layer	2.2E-6	0.013	
vertical MoSe ₂ aligned layer	2E-6	0.014	
[Mo ₃ S ₄] ⁴⁺ cluster	2.2E-7	0.07	35

References in Supporting Information

1. M. Tosun, D. Fu, S. B. Desai, C. Ko, J. Seuk Kang, D. H. Lien, M. Najmzadeh, S. Tongay, J. Wu and A. Javey, *Sci. Rep.*, 2015, **5**, 1-8.
2. S. Ding, X. Xiao, S. Liu, J. Wu, Z. Huang, X. Qi and J. Li, *Appl. Phys. A*, 2019, **125**, 1-7.
3. D. G. Kvashnin, P. B. Sorokin, J. Brüning and L. A. Chernozatonskii, *Appl. Phys. Lett.*, 2013, **102**, 183112.
4. S. Chen, S. Kim, W. Chen, J. Yuan, R. Bashir, J. Lou, A. M. Van Der Zande and W. P. King, *Nano Lett.*, 2019, **19**, 2092-2098.
5. Y. H. Hung, A.-Y. Lu, Y. H. Chang, J. K. Huang, J. K. Chang, L.-J. Li and C. Y. Su, *ACS Appl. Mater. Interfaces.*, 2016, **8**, 20993-21001.
6. Y. Pak, Y. Kim, N. Lim, J. W. Min, W. Park, W. Kim, Y. Jeong, H. Kim, K. Kim and S. Mitra, *APL Mater.*, 2018, **6**, 076102.
7. Y. Li, E. C. Moy, A. A. Murthy, S. Hao, J. D. Cain, E. D. Hanson, J. G. DiStefano, W. H. Chae, Q. Li and C. Wolverton, *Adv. Funct. Mater.*, 2018, **28**, 1704863.
8. Z. Wang, X. Zhang, J. A. Hachtel, A. Apte, C. S. Tiwary, R. Vajtai, J. C. Idrobo, R. Ozturk and P. Ajayan, *Nanoscale Horiz.*, 2019, **4**, 689-696.
9. A. Aljarb, J. H. Fu, C. C. Hsu, C. P. Chuu, Y. Wan, M. Hakami, D. R. Naphade, E. Yengel, C. J. Lee and S. Brems, *Nat. Mater.*, 2020, **19**, 1300-1306.
10. S. Hu, J. Li, X. Zhan, S. Wang, L. Lei, Y. Liang, H. Kang, Y. Zhang, Z. Chen and Y. Sui, *Sci. China Mater.*, 2020, **63**, 1065-1075.
11. S. Li, Y. C. Lin, W. Zhao, J. Wu, Z. Wang, Z. Hu, Y. Shen, D. M. Tang, J. Wang and Q. Zhang, *Nat. Mater.*, 2018, **17**, 535-542.
12. R. Zhang, M. Zhang, H. Yang, G. Li, S. Xing, M. Li, Y. Xu, Q. Zhang, S. Hu and H. Liao, *Small Methods*, 2021, **5**, 2100612.
13. J. Zhu, Z. C. Wang, H. Dai, Q. Wang, R. Yang, H. Yu, M. Liao, J. Zhang, W. Chen and Z. Wei, *Nat. Commun.*, 2019, **10**, 1-7.
14. Z. Wang, Q. Li, H. Xu, C. Dahl-Petersen, Q. Yang, D. Cheng, D. Cao, F. Besenbacher, J. V. Lauritsen and S. Helveg, *Nano Energy*, 2018, **49**, 634-643.
15. J. Xu, G. Shao, X. Tang, F. Lv, H. Xiang, C. Jing, S. Liu, S. Dai, Y. Li and J. Luo, *Nat. Commun.*, 2022, **13**, 1-8.
16. H. Li, C. Tsai, A. L. Koh, L. Cai, A. W. Contryman, A. H. Fragapane, J. Zhao, H. S. Han, H. C. Manoharan and F. Abild-Pedersen, *Nat. Mater.*, 2016, **15**, 48-53.
17. S. Su, Q. Zhou, Z. Zeng, D. Hu, X. Wang, M. Jin, X. Gao, R. Nötzel, G. Zhou and Z. Zhang, *ACS Appl. Mater. Interfaces.*, 2018, **10**, 8026-8035.
18. G. Ye, Y. Gong, J. Lin, B. Li, Y. He, S. T. Pantelides, W. Zhou, R. Vajtai and P. M. Ajayan, *Nano Lett.*, 2016, **16**, 1097-1103.
19. A. D. Nguyen, T. K. Nguyen, C. T. Le, S. Kim, F. Ullah, Y. Lee, S. Lee, K. Kim, D. Lee and S. Park, *ACS omega*, 2019, **4**, 21509-21515.
20. Q. Zhou, X. Luo, Y. Li, Y. Nan, H. Deng, E. Ou and W. Xu, *Int. J. Hydrot. Energy*, 2020, **45**, 433-442.
21. Q. Zhou, S. Su, P. Cheng, X. Hu, X. Gao, Z. Zhang and J. M. Liu, *J. Mater. Chem. C*, 2020, **8**, 3017-3022.
22. J. Pető, T. Ollár, P. Vancsó, Z. I. Popov, G. Z. Magda, G. Dobrik, C. Hwang, P. B. Sorokin and L. Tapasztó, *Nat. Chem.*, 2018, **10**, 1246-1251.
23. A. Bala, A. Sen, Y. H. Kim, Y. M. Kim, S. Gandla, H. Park and S. Kim, *J. Phys. Chem. C*, 2022.
24. H. Y. Cho, T. K. Nguyen, F. Ullah, J. W. Yun, C. K. Nguyen and Y. S. Kim, *Phys. B: Condens. Matter.*, 2018, **532**, 84-89.
25. C. Tsai, H. Li, S. Park, J. Park, H. S. Han, J. K. Nørskov, X. Zheng and F. Abild-Pedersen, *Nat. Commun.*, 2017, **8**, 1-8.
26. J. Wang, M. Yan, K. Zhao, X. Liao, P. Wang, X. Pan, W. Yang and L. Mai, *Adv. Mater.*, 2017, **29**, 1604464.
27. Y. Wang, S. Udyavara, M. Neurock and C. D. Frisbie, *Nano Lett.*, 2019, **19**, 6118-6123.
28. L. Tao, X. Duan, C. Wang, X. Duan and S. Wang, *ChemComm*, 2015, **51**, 7470-7473.
29. H.-Y. Cho, T. K. Nguyen, F. Ullah, J. W. Yun, C. K. Nguyen and Y. S. Kim, *Physica B: Condens. Matter.*, 2018, **532**, 84-89.

- Condensed Matter*, 2018, **532**, 84-89.
- 30. L. Tao, X. Duan, C. Wang, X. Duan and S. Wang, *ChemComm*, 2015, **51**, 7470-7473.
 - 31. B. Conway and B. Tilak, *Electrochimica acta*, 2002, **47**, 3571-3594.
 - 32. S. Trasatti, *J. electroanal. chem*, 1972, **39**, 163-184.
 - 33. T. F. Jaramillo, K. P. Jørgensen, J. Bonde, J. H. Nielsen, S. Horch and I. Chorkendorff, *science*, 2007, **317**, 100-102.
 - 34. D. Kong, H. Wang, J. J. Cha, M. Pasta, K. J. Koski, J. Yao and Y. Cui, *Nano Lett.*, 2013, **13**, 1341-1347.
 - 35. T. F. Jaramillo, J. Bonde, J. Zhang, B.-L. Ooi, K. Andersson, J. Ulstrup and I. Chorkendorff, *J. Phys. Chem. C*, 2008, **112**, 17492-17498.